DESIGN AND ANALYSIS OF CLOSED CIRCUIT LOW SPEED SUBSONIC WIND TUNNEL

Prakash Koirala, Rahul Jamkatel and Shahil Sharma

ABSTRACT

This paper aims to provide a complete design methodology for a subsonic closed circuit wind tunnel with an axial fan and flow analysis using CFD simulations for the designed wind tunnel. The methodology starts with establishing the relation of various geometrical and loss parameters of both wind tunnel channel and axial fan using analytical methods. A wind tunnel having test section dimensions of 2.6 m width and 1.84 m height with operating test section velocity of 100 m/s was designed with low turbulence considerations. Then CFD simulations of the channel and axial fan were performed separately to analyse the flow behaviour inside the wind tunnel. The analytically calculated loss parameters of channel and pressure rise provided by fan was compared with the results obtained from CFD simulations. The maximum velocity at the test section obtained from CFD was 103.251 m/s. The designed wind tunnel achieved deviation of flow uniformity within 1% in mid plane of test section and turbulence intensity less than 0.17%. The total pressure loss coefficient from simulation was 16.34% greater than that from analytical calculations. Simulations for test section velocity of 20 m/s and 50 m/s were also performed which yielded similar flow quality in test section as 100 m/s simulation. It provided the operating range of 20 − 100 m/s for the designed wind tunnel. By implementing the isolated airfoil theory for blade element design and free vortex assumption for three-dimensional flow equilibrium, a single-stage axial fan with stage efficiency of 89% and pressure rise of 887 Pa was designed. The total pressure difference of 853 Pa was achieved from CFD simulation of axial fan with an efficiency of 80.85%, which is an acceptable result in the case of single stage axial fan. The obtained CFD result of pressure rise was 3.8% deviated from pressure rise requirement.

Methodology

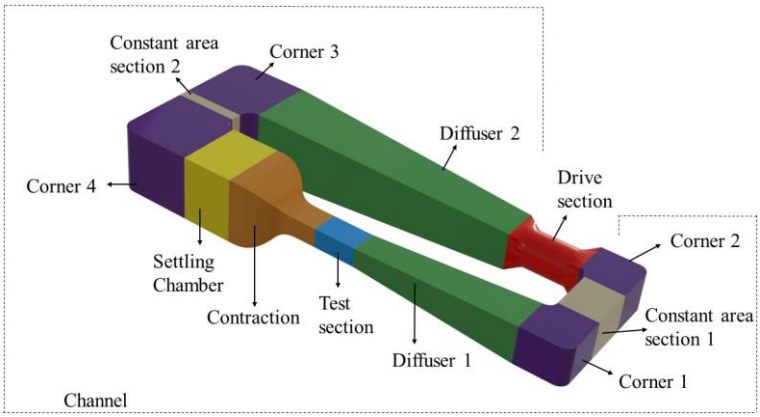

Figure: Components of closed wind tunnel

The methodology followed for calculating the geometrical and loss parameters of each component of the closed-circuit wind tunnel (see Figure 1) has been discussed in this section. The wind tunnel can be divided into two groups; channel and drive section. Figure 2 shows a sequential design methodology for closed circuit low speed subsonic wind tunnel.

As the air flows from drive section to different components of channel circulating back to it, pressure losses occurs at each components of channel. The nondimensionalization of these pressure losses with the dynamic pressure at the entrance of these components gives the local loss coefficient of the individual component of the channel ($K_{component}$). The local loss coefficient with respect to the test section ($Ktest_{component}$) were then calculated by using the formula as given below:

$$Ktest_{component} = K_{component} \times \left(\frac{A_{ts}}{A}\right)^2 \quad (1)$$

where A and A_{ts} are the smallest cross section area of components and cross section area of test section. The reciprocal of sum of these loss coefficients with respect to test section gives Energy ratio (E_R) of wind tunnel as given by the equation below:

$$E_R = \frac{P_{ts}}{P_c} = \frac{1}{\Sigma Ktest_{component}} \quad (2)$$

Energy ratio is the measure of efficiency in terms of flow energy and can also be defined as the ratio of power of flow in the test section (P_{ts}) to power loss throughout the channel (P_c) as shown in Equation 2. It is typically in the range of 3-7 for closedcircuit wind tunnel (Barlow, Rae, & Pope, 1999). Energy ratio and volume flow rate at test section from channel serves as input for the calculation of pressure rise (ΔP) to be provided by axial fan. This pressure rise compensates for the total loss of pressure in the channel and is the design requirement for the design of axial fan in drive section which is further discussed in the later section.

In the test section, evaluation of flow quality is essential as it determines the suit-

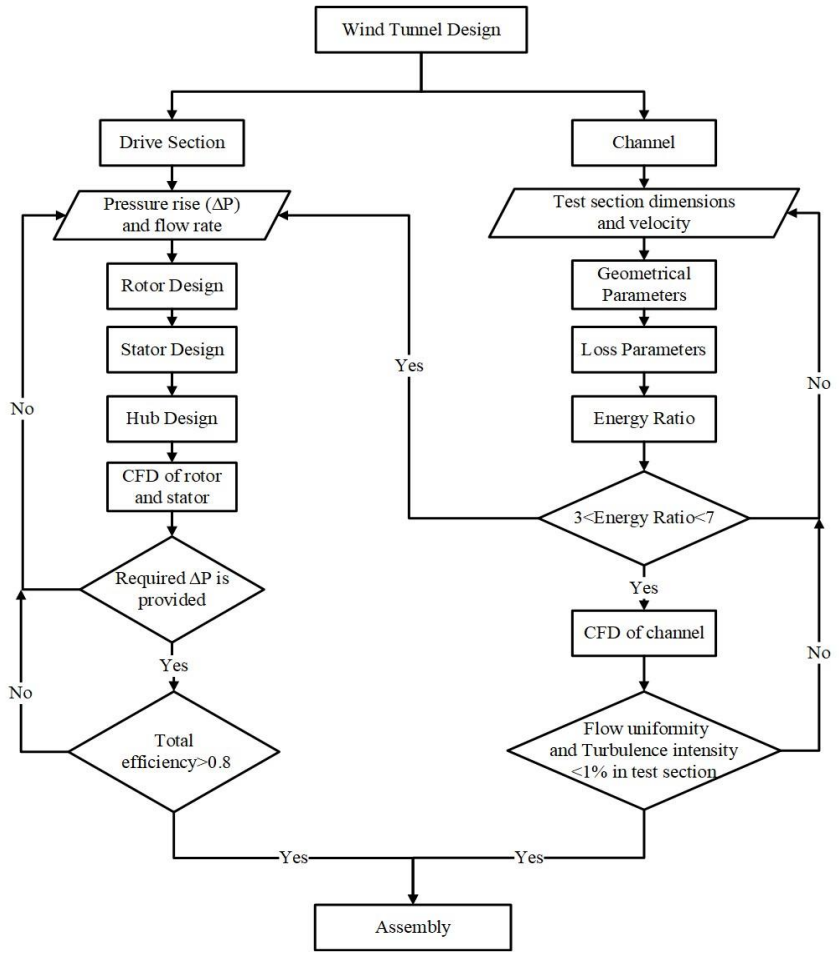

Figure: Wind Tunnel Design Methodology

ability of wind tunnel for different types of applications. At the test section, flow quality can be observed in the form of flow uniformity and turbulence intensity. Flow uniformity of test section is velocity at a point divided by the maximum velocity at test section i.e. U/U_{max}. The deviation in flow uniformity shows how much the flow is uniform at different points with respect to the maximum velocity achieved. Turbulence intensity can be defined as standard deviation of velocity fluctuations to reference mean flow velocity and is a characterization of turbulence level in wind tunnel. Turbulence intensity below 1% is often classified as low turbulence case. The channel design should achieve required uniformity of average air velocity along with turbulence intensity in the test section depending on the wind tunnel applications. For a general purpose wind tunnel, deviation in flow uniformity of average air velocity and turbulence intensity should be below 1% in the test section (Balendra, Shah, Tey, & Kong, 2002; Moonen, Blocken, Roels, & Carmeliet, 2006). These flow quality parameters will be assessed using CFD simulations of channel.

CFD Methodology

The aerodynamic behaviour of the designed wind tunnel was assessed by performing CFD analysis separately for channel and drive section. CFD analysis was performed to verify whether the designed wind tunnel with dimensions obtained from analytical calculations achieves the design requirements of channel and drive section. Also, the flow quality at different locations were observed.

Due to symmetrical nature of channel geometry over the mid plane in height wise direction, only half of the channel was required to be modelled for CFD analysis which reduced computational resources required. Simulation of entire channel components was performed rather than conventional technique (simulating the test section only) as it showed 2-4 times better results than conventional technique and good agreement with experimental results. (Moonen et al., 2006). Mesh generation of the model was done using hybrid meshing strategy in POINTWISE. Unstructured meshing was carried out for corners as it consisted of corner vanes which complicated the geometry and structured meshing was done for all other components of channel (see Figure 9). The corner vanes also had structured boundary layer mesh. Channel model with different mesh sizes were evaluated to check the dependence of the CFD solution with mesh size for same solution methods and boundary conditions.

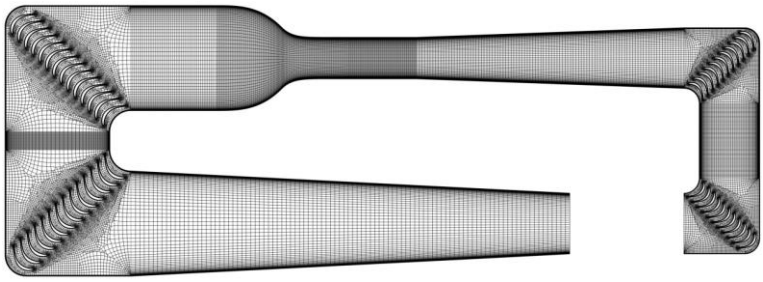

Figure: Meshing of Channel

The steady state computational fluid analysis of the model was performed by solving 3D RANS equations using ANSYS FLUENT. Standard $k-\epsilon$ turbulence model with Standard wall functions were selected for turbulence kinetic energy and dissipation rate. Calautit, Chaudhry, Hughes, and Sim (2014) showed standard $k-\epsilon$ to be the most suitable for predicting test section flow speed and turbulence intensity as it had better correlation with experimental results compared to $k-\omega$ and Reynolds stress turbulence models. SIMPLEC velocity-pressure coupling algorithm was employed along with the second order pressure interpolation and QUICK Discretization Scheme for turbulence and momentum equations.

For boundary conditions, velocity inlet of 33.3 *m/s* was applied to inlet of Diffuser 2 and outlet zero gauge pressure was applied to exit of Corner 2. This approach of using inlet velocity as boundary condition was also applied by Bertholds (2012) and Almeida, Miranda, Ferreira Neto, and Saad (2018). Stationary wall and symmetry boundary conditions were applied to the walls of channel and bottom surface of half model of channel respectively. The residuals were set to converge at 10^{-4}.

As stated earlier the analysis of axial fan was performed separately from channel for which the CAD model of fan rotor blade was generated by stacking the blade element at nine different sections radially for the smooth twist of the blade. Similarly, stator blade element was stacked radially by aligning zero lift line (chord line for symmetrical airfoil used) parallel

to the axis of rotation. Then, the flow paths around the blades and setup for meshing were defined using ANSYS BLADE MODELER and ANSYS TURBOGRID for meshing. All the methods and parameters were controlled and set in such a way that there was no error in the mesh. To check the dependence of the CFD results with mesh size, mesh independence test was performed with five different meshes. All meshes were simulated with same solution methods and boundary conditions. The mesh was refined until the difference in pressure raise value of two consecutive mesh was minimum. Velocity inlet of 71.68 *m/s* and outlet gauge pressure

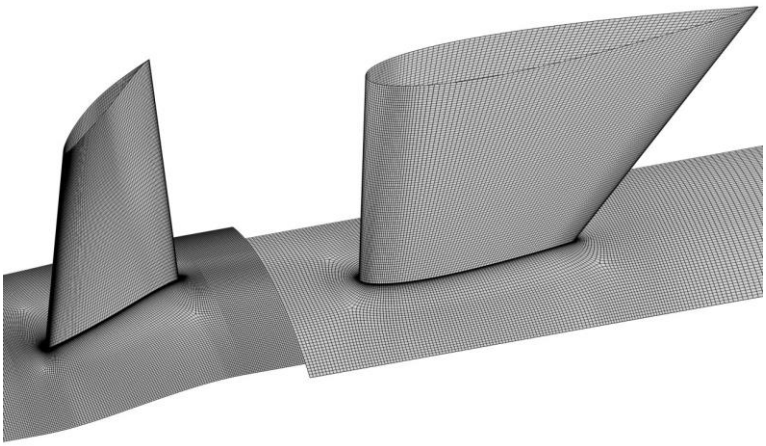

Figure: Meshing of rotor and stator

of 0 *Pa* was applied at inlet of rotor and outlet of stator respectively. The wall type boundary condition was imposed at hub, shroud and blade. The rotor was set as rotating domain with a rotational speed of 450 *rpm* and stator domain was set as stationary domain. The mixing plane interface was used between rotor and stator domain as this model shows the closer results to experimental data than the frozen rotor model (Le Roux, 2010). The stage interface (mixing plane interface) takes the circumferential average of the fluxes through bands on the interface. Any of the flow quantities or any irregularities (wakes and separation) were averaged circumferentially at this interface prior to entry towards the stator domain. This results in uniform pressure and velocity circumferentially and this model is widely used in multi stage machines between the domains of each stage and consumes more computational effort than the frozen rotor model (Andreadis, 2011).

Most of the researchers used k–ϵ as the turbulence model and also on performing the simulation using both k–ϵ and Shear Stress Transport model the results obtained were similar. Hence k–ϵ turbulence model was used and turbulence intensity was assumed to be 5%. In the solver option, the advection scheme was first set to high resolution and simulation was performed but the solution did not converge. So, upwind advection scheme and high resolution turbulence numerics were used to solve the model. The convergence was controlled using maximum number of iteration of 10000 and physical timescale of 1×10^{-4}. The RMS residual target was set to 1×10^{-5} for convergence criteria. With the mentioned methodology the analysis of both the channel and the axial fan was performed and the results were obtained.

Results and Discussion

5.1. Geometrical and loss parameters of channel

Following the design methodology, the overall dimensions of a closed-circuit wind tunnel with a rectangular test section of width 2.6 *m* and height 1.84 *m* along with maximum operating speed of 100 *m/s* was calculated . Also, the maximum achievable Reynold's number was 1.4756×10^7. The geometrical parameters and loss coefficients of each component with respect to test section ($Ktest_{component}$) of wind tunnel are presented in Table 1. It was observed that Diffuser 1 contributed the most in the total loss coefficient of 50.5%, followed by Corner 1 (12.2%) and Corner 2 (10.5%). The four corners covered 27.2% of the total loss coefficient in the channel. Hence, Energy ratio (E_R) of the wind tunnel calculated (excluding honeycomb and screen combinations) was 6.90, which lies within the suitable E_R range of 3-7 suggested by Barlow et al.
(1999).

Table 1. Geometrical and loss parameters of channel

Components of channel	Inlet Width (*m*)	Inlet Height (*m*)	Outlet Width (*m*)	Outlet Height (*m*)	Length (*m*)	θ (°)	*rc* (*m*)	*Ktestcomponent*
Test section	2.60	1.84	2.60	1.84	4.31			0.0153
Contraction	6.56	6.56	2.60	1.84	8.20			0.0101
Diffuser 1	2.60	1.84	3.79	3.79	16.68	2.707		0.0732
Corner 1	3.79	3.79	3.79	3.79			0.95	0.0177
Constant sec-area tion 1	3.79	3.79	3.79	3.79	4.61			0.0011
Corner 2	3.79	3.79	3.79	3.79			0.95	0.0177
Diffuser 2	3.79	3.79	6.56	6.56	27.38	2.90		0.0057
Corner 3	6.56	6.56	6.56	6.56			1.31	0.0020
Constant sec-area tion 2	6.56	6.56	6.56	6.56	1.12			0.00002
Corner 4	6.56	6.56	6.56	6.56			1.31	0.0020
Settling Chamber	6.56	6.56	6.56	6.56	5.32			0.0001
Total loss coefficient w.r.t test section								0.1449

The loss coefficients of honeycomb and screens were not included in calculation of E_R in order to compare the analytical results with CFD results. Incorporating honeycomb and screen arrangement in CFD model would require tremendously high computing power. After the exclusion of the honeycombs and screen, value of loss coefficient of Settling Chamber was obtained by considering it as a constant area section. However, this design consists of one honeycomb and three screens arrangement installed in Settling chamber, which are separated 1.31 *m* apart. The geometrical and loss parameters for honeycomb and screen are provided in Table 2.

Table 2. Geometric and loss parameters for honeycomb and screens

Description	Value
Single cell diameter - inscribed circle (d_h)	10.92
Number of divisions in height wise direction (n_{height})	332
Number of divisions in width wise direction (n_{width})	1065
Length of honeycomb (L_h)	69
Local loss coefficient of honeycomb ($K_{honeycombs}$)	0.2590
Number of wires in each direction (n_w)	mm 1420 mm m) mm
Screen mesh density (ρ_m)	216.38 (per
Screen mesh division (w_m)	4.62
Local loss coefficient of screen ($K_{screens}$)	0.5152
Total lateral turbulence reduction factor of screens ($f_{lateral}$)	0.7136
Total axial turbulence reduction factor of screens (f_{axial})	0.0130

5.2. Geometrical and loss parameters of Axial Fan

Following the described methodology and with certain basic assumptions, various design parameters for the axial fan were calculated. Table 3 and 4 summarizes the analytically calculated design parameters for rotor and stator respectively. These parameters were calculated at hub, mid and tip sections of the blade along the radial direction. The fan was designed in such a way that lift coefficient calculated analytically lies in the range designed lift of the selected airfoil and the angle of attack was selected at the maximum C_L/C_D. Also the suitable combination of the lift coefficient and solidity was maintained. The stator vanes were designed such a way that there is no swirl component of velocity behind the stator vanes.

Table 3. Basic parameters for rotor design

Design parameters	Hub section	Mid section	Tip section
Radius (r) in m	0.959	1.352	1.745
Rotor speed (U) in m/s	55.28	77.89	100.51
Pressure rise coefficient (K_{th})	0.317	0.317	0.317
Flow coefficient (λ)	1.584	1.124	0.872
Swirl coefficient (ϵ)	0.251	0.178	0.138
Inlet relative flow angle (β_1)	32.25°	41.64°	48.92°
Outlet relative flow angle (β_2)	20.80°	35.41°	45.26°

Mean relative flow angle (β_m)	26.81°	38.66°	47.15°
Solidity (σ)	0.69	0.49	0.38
Lift coefficient (C_L)	0.64	0.56	0.49
Angle of attack (α)	2.75°	2.75°	2.75°
Stager angle (ζ)	24.06°	35.91°	44.40°
Rotor chord (c_r) in *m*	0.524	0.524	0.524
Rotor loss coefficient(R_S)			0.04595

Table 4. Basic parameters for stator design

Design parameters	Hub section	Mid section	Tip section
Radius (r) in *m*	0.959	1.352	1.745
Swirl coefficient (ϵ)	0.251	0.178	0.138
Mean flow angle (α_m)	7.15°	5.09°	3.95°
Lift coefficient ($^{C}{}_{L}(stator)$)	0.50	0.35	0.28
Stator chord (c_s) in m	0.670	0.944	1.218
Stator loss coefficient (K_S)			0.06387

Furthermore, various losses at the rotor and stator were calculated and it was observed that 45% of the total loss was encountered at the rotor section while 55% was in the stator region. The losses at the stator could be improved using the cambered airfoil rather than symmetrical airfoil but would also increase the cost and complication in design process . With these losses the total analytical efficiency of axial fan was obtained to be 89% as the converged value. The torque of 10121.54 *Nm* and thrust of 5237.39 *N* was generated by the rotor.

5.3. Channel Simulation

To check the dependence of the CFD solution on mesh size, 4 different meshes: Mesh 1 (4,669,308 cells), Mesh 2 (5,143,726 cells), Mesh 3 (6,212,759 cells) and Mesh 4 (8,179,819 cells) were considered. With the same solution methods and boundary conditions applied for all four meshes, simulations were performed and the deviation from analytical test section velocity i.e., 100 *m/s* is shown in percentage (Figure 11). It shows that all the four meshes have maximum velocity above 103 *m/s* along with maximum deviation of 3.48% for Mesh 2. As there wasn't any significant change in deviation between Mesh 3 and Mesh 4, further mesh refinement wasn't considered to be necessary. Thus, the results of Mesh 4 with maximum test section velocity deviation of 3.251% was selected for further post processing.

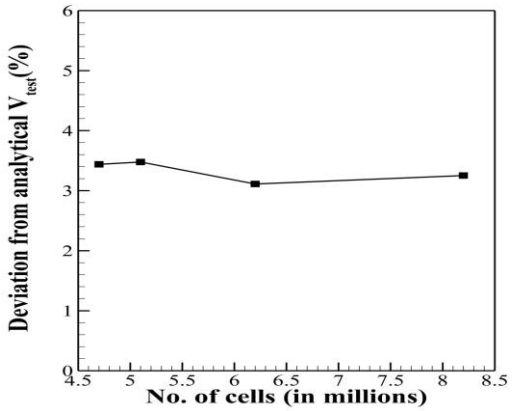

Figure: Mesh independence test of channel

Mesh 4 has maximum equiangle skewness of 0.688 and equiarea skewness of 0.827 which are within acceptable range. For boundary layer mesh resolution, the first cell height from the walls of channel was 0.002 *m* and from the corner vanes was 0.001 *m*. This resulted in average wall Y plus of 230 in the test section, which was comparable with that obtained by Moonen et al. (2006) (250) and Calautit et al. (2014) (222.3).

The results from converged solution provided maximum test section velocity of 103.251 *m/s* and the total pressure loss of 1070.62 *Pa* in the channel. Figure 12 shows the velocity contour along with the velocity vectors at different sections of the horizontal symmetry plane of the channel. It is evident that flow separation doesn't exist in the whole channel, however boundary layer thickens at the downstream end of Diffuser 1, which continues till Corner 2. The wake of corner vanes seem to decrease in the constant area section as expected and significantly disappear going further.

Figure 13 shows the variation in cumulative loss coefficient with respect to test section between analytical solution and simulation results for all the components of wind tunnel channel. The components in horizontal axis are placed in a manner that it represents the flow of air as in wind tunnel simulation boundary conditions starting from Diffuser 2 and ending at Corner 2. The loss coefficient curve for simulation results evidently lies completely above the loss coefficient curve of analytical solution

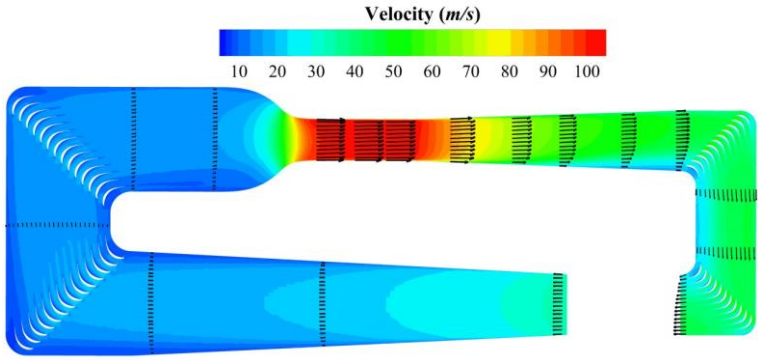

Figure: Velocity contour of channel at symmetry

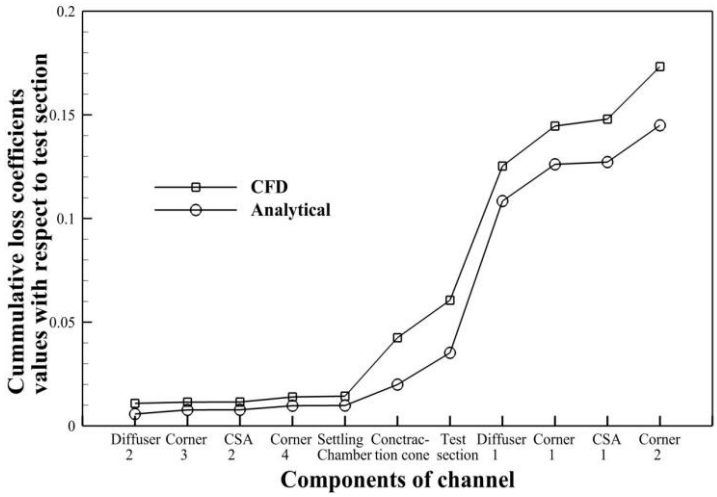

Figure: CFD vs Analytical Pressure loss coefficients

hence showing that analytical solution underestimated the loss coefficient for most of the components as compared to simulation results. Both analytical and simulation results show higher loss coefficient for components with higher flow velocity which is as expected as loss is proportional to square of velocity. The total pressure loss coefficient from simulation was 16.34% greater than that from analytical calculations. Three different locations of test section; Inlet, Mid section and Outlet were selected for assessing the flow quality at test section (see Figure 14).

Flow quality at the test section was observed in the form of flow uniformity and turbulence intensity both in widthwise and heightwise directions at Inlet, Mid plane and Outlet of test section as shown in Figures 15 and 16. Flow at Mid plane of test section was within 1% deviation of flow uniformity for both widthwise and heightwise direction. For Inlet and Outlet sections, flow was within 3% deviation of flow uniformity. The values obtained for flow uniformity from simulation were satisfactory as models are to be tested in the Mid plane section and required flow uniformity level is achieved at this section.

The turbulence intensity level was less than 0.17% at all specified locations. Turbulence intensity was seen to be minimum at the Mid plane compared to Inlet and Outlet of test section and turbulence intensity also seem to increase when approaching walls for widthwise direction which may be due to corner vanes of Corner 4 being at varying distance from test section. Turbulence intensity was obtained as low as 0.05% in the

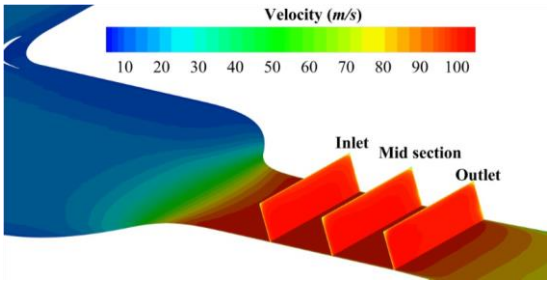

Figure: Cut sections of test section

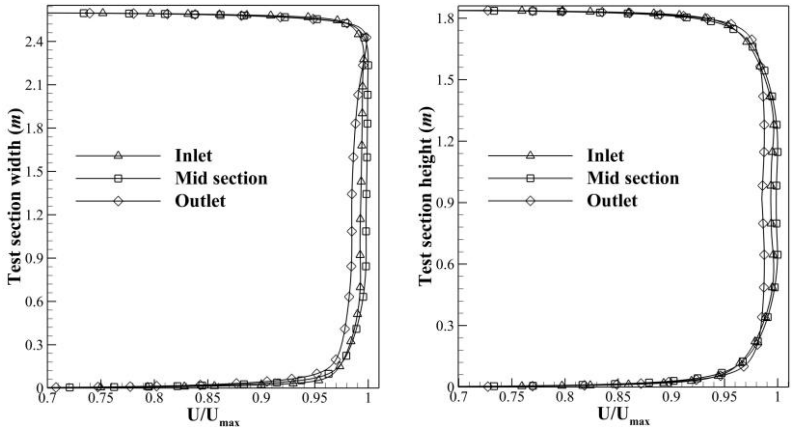

(a) Along widthwise direction (b) Along heightwise direction

Figure: Flow uniformity of test section

mid plane of test section. It showed that the designed wind tunnel is low turbulence wind tunnel as the turbulence intensity was below 1% in the test section.

To define the operating range of channel, simulations were also carried out for test section velocities of 20 *m/s* and 50 *m/s*. The flow uniformity and turbulent intensity was evaluated along the Mid plane along widthwise direction for velocities 20 *m/s*, 50 *m/s* and 100 *m/s* to observe the flow behaviour on reducing the test section velocity. It was observed that the behaviour of flow uniformity was significantly similar for all three test section velocities and turbulent intensity was below 0.17% in general. It implies that the designed channel performs well for these test section velocities and can be used for operating range of $20 - 100$ *m/s*.

5.4. Axial fan simulation

The designed modeled of axial fan was set for mesh independence test performed with five different meshes: Mesh 1 (441,462 cells), Mesh 2 (654,355 cells), Mesh 3 (1,043,312 cells), Mesh 4 (2,030,896 cells) and Mesh 5 (3,299,456 cells) to check the dependence of the results with mesh size. All meshes were simulated with same solution methods and boundary conditions. The analysis of the results of mesh independence test showed that Mesh 1 had least pressure rise of 801 *Pa* and highest deviation of 9.7% from analytical pressure rise while Mesh 5 had the highest pressure rise of 853 *Pa* and lowest deviation of 3.8% (see Figure 17). As there was no significant change in pressure rise and deviation between Mesh 4 and Mesh 5, so further refinement of mesh was not

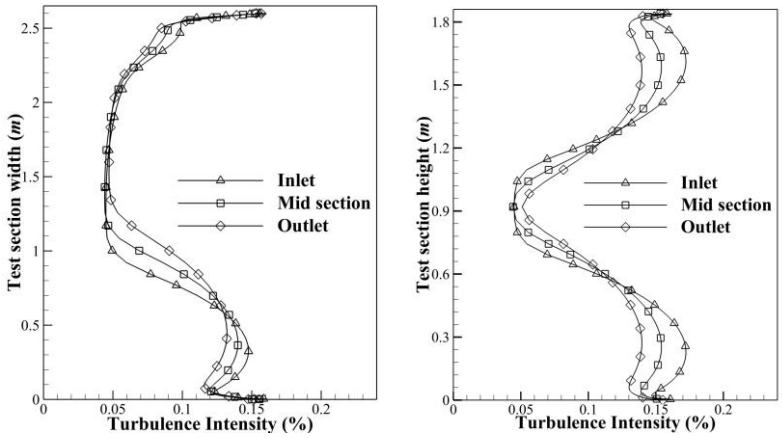

(a) Along widthwise direction (b) Along heightwise direction

Figure: Turbulence intensity in test section

necessary. Hence, the results of Mesh 5 was selected for further post processing.

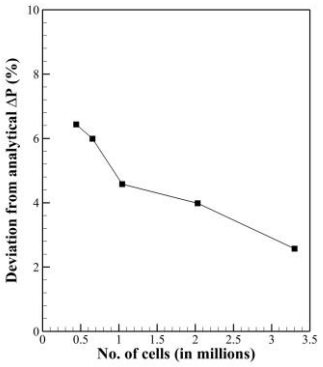

Figure: Mesh independence test of axial fan

After the convergence of the simulation for Mesh 5, the total pressure rise of 853 *Pa* at volumetric flow rate of 478.4 m^3/s from inlet to outlet of the fan section was obtained. The variation of total pressure from inlet to outlet of the domain is shown in Figure 18. The total pressure rise was contributed by rotor only keeping the rothalphy constant. Thus, the graph shows the rapid increase of the total pressure in the rotor region. In the case of an ideal stator, the total pressure remains constant however, this wasn't observed in Figure 18, where the total pressure in the stator gradually decreased. This occurs due to the fact that stator does not behave ideally so there was certain amount of loss in the stator, which caused gradual decrease in the total pressure. The pressure contour at the mid span of the axial fan indicating pressure rise moving from inlet to outlet is shown in Figure 19. The pressure variation on the suction side i.e. low pressure side, pressure side i.e. high pressure side and stagnation point are clearly visible in both rotor and stator with the red spot near the leading edge.

From CFD, the calculated total pressure rise across the rotor of 974 *Pa* and the total pressure across the stage (rotor and stator) of 853 *Pa* was obtained with an stage efficiency of 80.85%. Analytically, the total pressure rise across the stage was calculated as 887 *Pa* with total stage efficiency of 89.0%. The deviation of the CFD

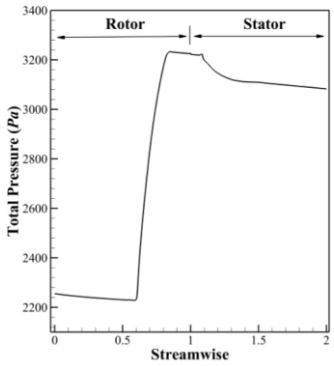

Figure 18. Inlet to Outlet Total Pressure rise

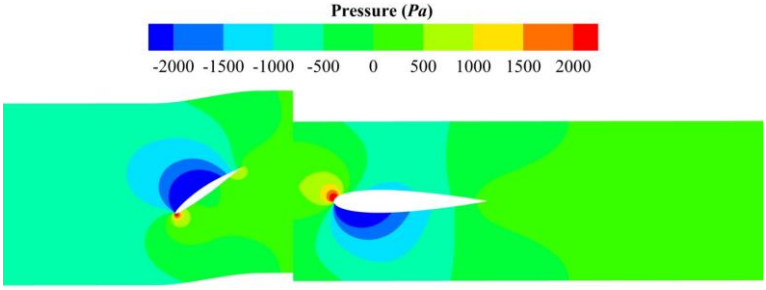

Figure 19. Pressure contour of axial fan at mid section

result from the analytical pressure rise was 3.8%. It can be attributed to the fact that the analytical calculation does not consider all the factors causing losses such as 3D losses due to airfoil, turbulent losses, tip clearance loss and hub, shroud and wall interaction losses however, these are considered in the CFD analysis.

Then, flow quality at the rotor and stator was visualized at different sections: Near Hub at 20% span, Mid span at 50% span and Near Tip at 80% span using vector plots as shown in Figure 20. It was observed that there was no any back flow and flow separation for rotor and stator blade at all three sections. The maximum velocity was observed at tip of the rotor blade in the suction side was 130.36 *m/s*, which is below 167 *m/s* as suggested by Wallis (1961).

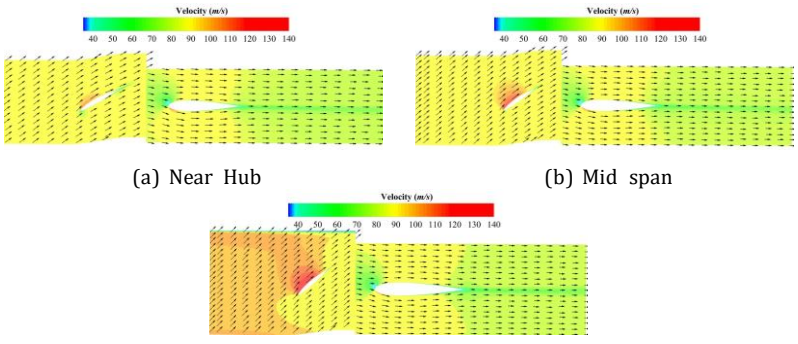

Figure 20. Velocity contour with vector at different span

Figure 21a, 21b and 21c represent the blade loading chart for Near Hub, Mid span and Near Tip of rotor blade respectively. Blade loading curve shows the pressure profile on the blade surface (both the pressure and the suction surface). The curve of the pressure side doesn't intersect the curve of the suction side, which is desirable for rotor blades. For axial fan, the lift force generated due to rotation of the rotor does work on the fluid to generate the pressure distribution as shown by the blade loading chart. The area between suction and pressure line also shows the amount of torque required to generate the pressure difference. It can be seen that the lift near the leading edge would contribute more to the total pressure difference created than that of trailing edge.

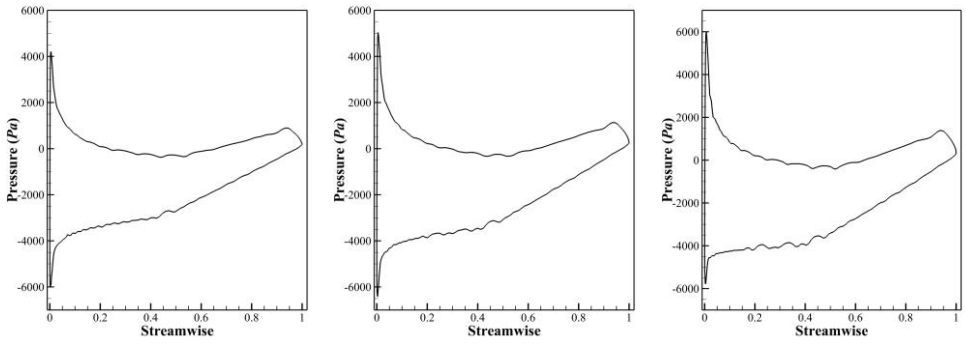

(a) Near Hub (b) Mid span (c) Near Tip

Figure 21. Rotor Blade Loading Chart

With the help of pressure contour on blade surfaces (both suction and pressure side) as shown in Figure 22, it was observed that the parallel strips of the pressure on suction and pressure side along the radial direction shows almost no variation in pressure. This phenomena exhibits that there is no significant radial flow and supports the free vortex theory used.

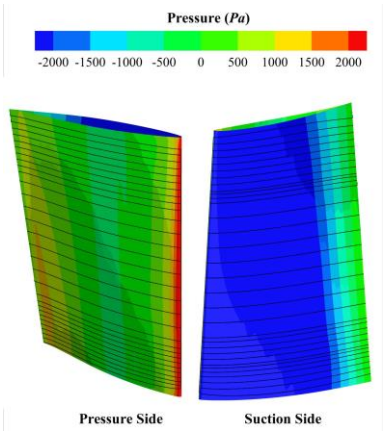

Figure 22. Pressure and suction side of rotor

Conclusions

A complete methodology for designing a closed circuit subsonic wind tunnel was developed. With the application of this methodology, wind tunnel with test section of 2.60 × 1.84 *m* and

maximum test section velocity of 100 *m/s* was designed. Using analytical methods, overall dimensions and loss coefficients for each component was calculated that yield Energy ratio of 6.9. For this obtained Energy ratio, a single stage axial fan was designed by implementing the isolated airfoil theory for blade design and free vortex flow for three-dimensional flow equilibrium.

The flow behaviour of the designed wind tunnel was assessed separately for channel and drive section using CFD simulations. The cumulative loss coefficients with respect to test section obtained from CFD for wind tunnel channel was higher when compared with that of analytically obtained values. Velocity contour with velocity vectors was observed at mid plane which exhibited no flow separation in the channel. Flow uniformity and turbulence intensity observed at Mid section of test section was less than 1 % deviation. In case of drive section, CFD result for total pressure rise across the stage was compared with that of numerical result and a deviation of 3.8% was obtained. Flow quality of rotor and stator was analysed using the velocity contour and vectors at near Hub, Mid span and near Tip and no flow separation and no vortex formation was observed. Thus the pressure rise generated by the designed axial fan can compensate the losses generated in the channel and maintain the required flow in the wind tunnel.

Disclosure Statement

On the behalf of all authors, the corresponding author declares that there is no conflict of interest.